A New variant of Van Leer's method for multidimensional systems of conservation laws

Benoît Perthame, Youchun Qiu

UNITÉ DE RECHERCHE
INRIA-ROCQUENCOURT

Institut National
de Recherche
en Informatique
et en Automatique

Domaine de Voluceau
Rocquencourt
B.P. 105
78153 Le Chesnay Cedex
France
Tél.:(1) 39 63 55 11

Rapports de Recherche

N° 1562

Programme 6
Calcul Scientifique, Modélisation et
Logiciel numérique par Ordinateur

A NEW VARIANT OF VAN LEER'S METHOD FOR MULTIDIMENSIONAL SYSTEMS OF CONSERVATION LAWS

Benoît PERTHAME
Youchun QIU

Novembre 1991

RR_1562

A NEW VARIANT OF VAN LEER'S METHOD FOR MULTIDIMENSIONAL SYSTEMS OF CONSERVATION LAWS

Benoît Perthame (*) (**) - *Youchun Qiu* (**)

* Département de Mathématiques - Université d'Orléans, BP 6759, 45067 Orléans Cedex 2
** INRIA, Projet MENUSIN, BP 105, 78153 Le Chesnay Cedex.

ABSTRACT

We give a new interpretation of Van Leer's construction of second order accurate upwind schemes for hyperbolic systems of conservation laws. It consists in first interpolating values at the nodes of the mesh, then correcting them globally on each cell by a conservation argument. This leads to represent functions, no longer as piecewise linear, but as piecewise constant in subcells. It can be used on a rectangular, triangular or mediane based dual grid to get a genuinely multidimensional scheme, and also to prove that the second order scheme gives non negative values of the pressure and density for gas dynamics, even on an unstructured mesh. Thus this approach is very robust.

UNE NOUVELLE VARIANTE DE LA METHODE DE VAN LEER POUR DES LOIS DE CONSERVATIONS MULTIDIMENSIONNELLES

RESUME

Nous donnons une nouvelle interprétation de la construction de Van Leer de schémas décentrés d'ordre 2 pour les systèmes hyperboliques de lois de conservation. Nous interpolons d'abord la fonction aux noeuds du maillage, ensuite nous corrigeons globallement sur chaque maille les valeurs obtenues grâce à un argument de conservation. Ceci conduit à une représentation des fonctions, non plus linéairement par morceaux, mais constantes par sous-mailles. On peut ainsi traiter des maillages rectangulaires, triangulaires ou duaux et obtenir un schéma vraiment multidimensionnel. On montre que, pour la dynamique des gaz, le schéma préserve la positivité de la densité et la pression, même sur un maillage non structuré à l'ordre 2. Cette approche est donc très robuste.

Key words : upwind schemes - second order schemes - systems of conservation laws - dual mesh -
Mots clefs : schémas décentrés - schémas d'ordre deux - systèmes de lois de conservation - maillage dual.
AMS class. numbers 65M60 - 76M20 - 76K05

INTRODUCTION

Upwind schemes are now commonly used, on various structured or unstructured meshes, for multidimensional hyperbolic systems of conservation laws

$$(1) \qquad \partial_t U^k + \mathrm{div}_x F^k(U) = 0 \ , \ x \in \mathbb{R}^2, \ 1 \le k \le m, \ F^k(U) \in \mathbb{R}^2 \ .$$

(We will consider here, for simplicity, only two space dimensions). They are very efficient for shock wave computations but require to be second order accurate at least. This is usually achieved using Van Leer's method [14] which consists in representing the solution of (1) as a piecewise linear function with a gradient appropriately constructed through min-mod type of limitations. Various versions of this idea have been used combined with the calculation of fluxes by a Riemann Solver applied to the values of U, calculated at the middle of the edges of the mesh ; this yields the approximation of (1) by the formula

$$(2) \qquad U_i^{k,n+1} - U_i^{k,n} + \sigma_i \sum_p \ell_p F_p^k \cdot n_p = 0$$

where for a given cell C_i , the boundary ∂C_i is divided in edges E_p ($p = 1, \ldots, P$) of length ℓ_p and outer unit normal n_p . $F_p^k \cdot n_p$ is the value of the flux through the edge E_p and

$$(3) \qquad \sigma_i = \Delta t \ / \ \mathrm{area}\ (C_i) \ .$$

For this kind of finite volume approach we refer for instance to Collela [2], Sanders-Wieser [13], Durlofsky-Engquist-Osher [4], and the references therein.

In order to prove that the pressure cannot be negative for gas dynamics, to avoid the delicate question of slope construction and limitation especially on unstructured meshes when TVD criteria are not available, we propose another way to find the edge values to be used in the Riemann solver. It is based on the correction, by a conservation argument, of interpolated values at the nodes of the mesh. The main features of this approach, which is exactly a classical min-mod limitation in one dimension, are

i) We represent the solution by a piecewise constant by subcells function (see figures 1,2), and thus we are able to solve with few numerical errors the equation (1) if it is approximated by a linear equation as in the Boltzmann approach (see Deshpande [3], Perthame [9]), and at least we keep the theoretical properties of this approach.

ii) For rectangular grids we can take into account corners effects, but in fact the method diminish them even if the Riemann solver do not compute these effects, because the interpolated values, before the correction step are the same for all the cells around a node.

iii) For gas dynamics equations, we will prove that the second order scheme built in this way gives non-negative values of the density and of the pressure, even for an unstructured mesh.

iv) The correction we perform is global for the mesh (the interest of this seems clear in numerical experiments and has been pointed out several times) and is second order accurate under a general condition, (3), which applies to various type of meshes.

The paper is organized as follows : after a general description in section I, we describe the method more precisely for gas dynamics on a rectangular mesh (section II). The section III is devoted to the extension to an unstructured mesh of dual type and finally we present numerical results.

I. THE INTERPOLATION AND LIMITATION PROCEDURE.

In this section we present an interpolation procedure which gives, after a limitation step, a second order accurate evaluation of the fluxes in formula (2). After the description of the method, we prove that it is second order accurate in subsection I.3.

I.1. General description

Consider that the cells C_i of the computational domain are divided in subcells C_i^α with area s_i^α for $\alpha = 1, \ldots, \alpha_M$ ($\alpha_M = 3$ for triangles, $\alpha_M = 4$ for rectangles, but it could depend on the cell as in the case of the dual mesh presented in section III).

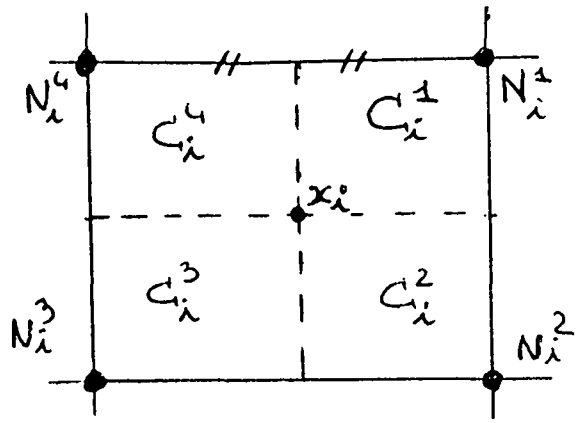

Figure 1. Subcell decomposition for a rectangular mesh.

Each of these subcells is supposed to contain one node of the mesh denoted by N_i^α when considering the cell C_i. Let x_i be the center of mass of the cell C_i, we assume

$$(3)\quad \sum_{\alpha=1}^{\alpha_M} s_i^\alpha N_i^\alpha = x_i \ , \ s_i^\alpha = \text{area}\ (C_i^\alpha) \ .$$

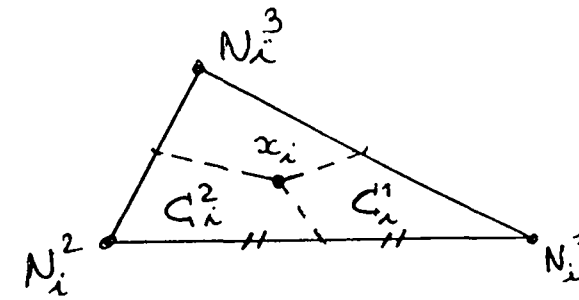

Figure 2. Subcell decomposition for a triangular mesh.

We are also given a piecewise constant function V_i on each cell C_i, related to the conserved quantities U_i by a non-linear relation $U^k = \Phi^k(V)$ (for gas dynamics we prefer to work on the quantities $V = (\rho, u_1, u_2, T)$ rather than $U = (\rho, \rho u_1, \rho u_2, E)$).

In order to compute a second order approximation of the fluxes around the cell C_i, we propose the following algorithm

i) Interpolate the cell values V_j to get a second order approximation $\hat{V}_i^\alpha$ of V at the node N_i^α and attribute this value to the subcell C_i^α so that the function V(x) is now piecewise constant on C_i.

ii) Apply a correction to the interpolated values $\hat{V}_i^\alpha$ such that the corrected values V_i^α satisfy the conservation relations

$$(4) \qquad \left(\sum_{\alpha=1}^{\alpha_M} s_i^\alpha \right) U_i^k = \sum_{\alpha=1}^{\alpha_M} \Phi^k(V_i^\alpha)\, s_i^\alpha \ .$$

iii) To complete the resolution of (1), apply an approximate Riemann solver to the various "sub-edges" of ∂C_i and apply (2).

Notice that the summation in the finite volume formula (2) is now performed over the edges of the subcells which belong to ∂C_i. Thus this procedure requires twice as many approximate Riemann problems as a classical reconstruction by edge. Therefore it should be done with a cheap solver ; below we will use a kinetic flux decomposition

Let us now detail a possible correction step to recover V_i^α from $\hat{V}_i^\alpha$ in the step (ii) above, in the special case of gas dynamics equations.

I.2. Limitation by conservation for gas dynamics

The compressible Euler Equations correspond to the case where, in (1),

$$(5)\ U = \begin{pmatrix} \rho \\ \rho u_1 \\ \rho u_2 \\ E \end{pmatrix}, \quad F_1(U) = \begin{pmatrix} \rho u \\ \rho u_1^2 + p \\ \rho u_1 u_2 \\ (E+p)u_1 \end{pmatrix}, \quad F_2(U) = \begin{pmatrix} \rho u \\ \rho u_1 u_2 \\ \rho u_2^2 + p \\ (E+p)u_2 \end{pmatrix},$$

and

$$(6)\ E = \rho\left(u_1^2 + u_2^2\right)/2 + \rho e \ , \ p = \rho T = (\gamma-1)\rho e, \text{ for some } \gamma,\ 1 < \gamma \leq 2 \ .$$

In this case we choose the physical variables $V = (\rho, u_1, u_2, T)$ to perform the interpolation and limitation procedure although, in general, the only choice seems to be the characteristic variables.

Then a possible correction step (ii) in subsection I.1. can be the following (we now drop the index i).

Conservation of mass.

Correct among the interpolated values $\hat{\rho}^\alpha$, those that are larger or smaller than the known average value ρ in the cell C_i in order to get conservation i.e.

$$(7) \qquad \rho^\alpha = \rho + \beta_+ (\hat{\rho}^\alpha - \rho)_+ - \beta_- (\hat{\rho}^\alpha - \rho)_-$$

where $0 \le \beta_-, \beta_+ \le 1$ are choosen such that either $\beta_+ = 1$ or $\beta_- = 1$ and $\sum_\alpha s^\alpha \rho^\alpha = \sum_\alpha s^\alpha \rho$:

$$(8) \qquad \beta_\pm = \text{Min}\left(1, \sum_\alpha s^\alpha \left(\hat{\rho}^\alpha - \rho\right)_{\mp} \Big/ \sum_\alpha s^\alpha \left(\hat{\rho}^\alpha - \rho\right)_{\pm}\right)$$

and $x_+ = \max(0,x)$, $x_- = \max(0, -x)$. This choice gives indeed $\sum_\alpha s^\alpha \rho^\alpha = (\sum s^\alpha)\rho$, which will be used in Section II.

Conservation of momentum

For $u = u_1$ or u_2 we set

$$(9) \qquad u^\alpha = u + \beta_+ \left(\hat{u}^\alpha - u\right)_+ - \beta_- \left(\hat{u}^\alpha - u\right)_- ,$$

with

$$(10) \qquad \beta_\pm = \text{Min}\left(1, \sum s^\alpha_\alpha \rho^\alpha \left(\hat{u}^\alpha - u\right)_{\mp} \Big/ \sum_\alpha s^\alpha \rho^\alpha \left(\hat{u}^\alpha - u\right)_{\pm}\right),$$

where ρ^α is the previously computed value of ρ in the subcell C^α. Notice that we get the conservation of momentum since from (9) and (10)

$$(11) \qquad \sum_\alpha s^\alpha \rho^\alpha u^\alpha = \sum_\alpha s^\alpha \rho^\alpha u = \left(\sum_\alpha s^\alpha\right)\rho u .$$

The same correction is applied to the two components of the velocity but it could more naturally be done in the local coordinates given by the vectors $(u_1 u_2)$ and $(u_1 u_2)^\perp$.

Conservation of energy.

Using ρ^α, u_1^α, u_2^α computed before, we set

$$(12) \qquad T^\alpha = T - (\gamma-1)\left[(u_1^\alpha - u_1)^2 + (u_2^\alpha - u_2)^2\right]/2 + \beta_+ \left(\hat{T}^\alpha - T\right)_+ + \beta_- \left(\hat{T}^\alpha - T\right)_-$$

where

$$(13) \qquad \beta_\pm = \mathrm{Min}\left(1,\ \Sigma_\alpha\, s^\alpha \rho^\alpha \left(\hat{T}^\alpha - T\right)_\mp \Big/ \Sigma_\alpha\, s^\alpha \rho^\alpha \left(\hat{T}^\alpha - T\right)_\pm\right) .$$

In order to prove that this is a conservative reconstruction, we compute using the conservation of mass and momentum,

$$\Sigma_\alpha\, s^\alpha \rho^\alpha \left(u_1^{\alpha 2} + u_2^{\alpha 2}\right)$$

$$= \Sigma_\alpha\, s^\alpha \rho^\alpha \left(\left(u_1^\alpha - u_1\right)^2 + \left(u_2^\alpha - u_2\right)^2 - u_1^2 - u_2^2 + 2u_1 u_1^\alpha + 2u_2 u_2^\alpha\right)$$

$$= \Sigma_\alpha\, s^\alpha \rho^\alpha \left(\left(u_1^\alpha - u_1\right)^2 + \left(u_2^\alpha - u_2\right)^2\right) + \Sigma_\alpha\, s^\alpha \rho \left(u_1^2 + u_2^2\right) .$$

therefore

$$\Sigma_\alpha\, s^\alpha \rho^\alpha \left[\left(u_1^{\alpha 2} + u_2^{\alpha 2}\right)(\gamma-1)/2 + T^\alpha\right]$$

$$= \Sigma_\alpha\, s^\alpha \rho \left(u_1^2 + u_2^2\right)(\gamma-1)/2 + \Sigma_\alpha\, s^\alpha \rho^\alpha T$$

$$= \Sigma_\alpha\, s^\alpha \rho \left[\left(u_1^2 + u_2^2\right)(\gamma-1)/2 + T\right] = \Sigma_\alpha\, s^\alpha E(\gamma-1) .$$

This proves the conservation of energy.

Remark : The idea that the temperature T has to be corrected by the value $(\gamma-1)\,|u|^2/2$ for positivity was introduced in [9] in 1D.

We now prove that this reconstruction gives non-negative values of ρ^α, T^α.

Theorem 1. If the interpolated values satisfy $\hat{\rho}^\alpha \geq 0$, $\hat{T}^\alpha \geq 0$ and

$$(14) \qquad (\gamma-1)\left(\hat{u}_1^\alpha - u_1\right)^2 \leq T \quad , \quad (\gamma-1)\left(\hat{u}_2^\alpha - u_2\right)^2 \leq T$$

for all $1 \leq \alpha \leq \alpha_M$, then the corrected values satisfy $\rho^\alpha \geq 0$, $T^\alpha \geq 0$.

Proof. Given α, the limitations (7) , (9), give

$$|u_1^\alpha - u_1| \leq |\hat{u}_1^\alpha - u_1| \quad , \quad |u_2^\alpha - u_2| \leq |\hat{u}^\alpha - u_2| \quad , \quad |\rho^\alpha - \rho| \leq |\hat{\rho}^\alpha - \rho|.$$

Since $\hat{\rho}^\alpha$ and ρ are non-negative this gives $\rho^\alpha \geq 0$. And (12) immediately gives $T^\alpha \geq 0$.

1.3. Second order accuracy (case of gas dynamics).

We conclude this section in proving that the complete reconstruction described in subsections I.1, I.2 is second order accurate in the smoothness regions.

Theorem 2. Assume that for all i the cell C_i is a polygon of vertices $\left(N_i^\alpha\right)_{1\leq\alpha\leq\alpha_M}$ devided in subcells C_i^α satisfying (3). If the interpolated values $\hat{V}_i^\alpha$ are second order approximations of the exact values $V\left(N_i^\alpha\right)$, then the corrected values V_i^α are also second order approximations of $V\left(N_i^\alpha\right)$.

Corollary 3. With the assumptions of theorem 2, for any pair of neighbor vertices $\left(N_i^\alpha,\ N_i^{\alpha+1}\right)$ the flux $\ell_\alpha\left(F\left(V_i^\alpha\right) + F\left(V_i^{\alpha+1}\right)\right)/2$ is a second order approximation of

$$\int_{\left(N_i^\alpha\ ,\ N_i^{\alpha+1}\right)} F\left(V(y)\right)\, d\sigma(y)$$

where $\sigma(y)$ denotes the Lebesgue measure or the edge $\left(N_i^\alpha, N_i^{\alpha+1}\right)$, $\ell_\alpha = |N_i^\alpha\ ,\ N_i^{\alpha+1}|$.

From corollary 2, it seems clear that the full scheme for (1) is formally second order accurate. Such a result is proved for a finite element method, using a regular unstructured grid, by Cockburn and Shu [16] for instance.

Proof of corollary 3. Since F is smooth and V is assumed to be smooth we have

$$F\left(V(y)\right) = \theta\, F\left(V\left(N_i^{\alpha}\right)\right) + (1-\theta)\, F\left(V\left(N_i^{\alpha+1}\right)\right) + O\left(\ell_{\alpha}^2\right) \text{ for}$$

$y = \theta\, N_i^{\alpha} + (1-\theta)\, N_i^{\alpha+1}$. Thus

$$\int_{\left(N_i^{\alpha},\, N_i^{\alpha+1}\right)} F\left(V(y)\right)\, d\sigma(y) = \frac{\ell_{\alpha}}{2}\left(F\left(V\left(N_i^{\alpha}\right)\right) + F\left(V\left(N_i^{\alpha+1}\right)\right)\right) + O\left(\ell_{\alpha}^3\right)$$

and using theorem 2, corollary 3 is proved.

Proof of theorem 2. The details of the proof are given in Y. Qiu [11] and we only sketch the main points. Since our limitation step is lipschitz continuous, it is enough to check that if $\rho(x)$ for instance is a linear function and $\hat{\rho}^{\alpha}$ are exact values, then the limitation step gives $\rho^{\alpha} = \hat{\rho}^{\alpha}$. In that case we have $\rho(x) = D\rho\cdot(x-x_i) + \rho(x_i)$, and because x_i is the center of mass of C_i we have $\rho_i = \rho(x_i)$. Thus

$$\Sigma_{\alpha} s^{\alpha}\left(\hat{\rho}^{\alpha} - \rho_i\right) = D\rho\cdot\Sigma_{\alpha} S^{\alpha}\left(N_i^{\alpha} - x_i\right) = 0$$

using (3). This means that

$$\Sigma_{\alpha}\, s^{\alpha}\left(\hat{\rho}^{\alpha} - \rho_i\right)_+ = \Sigma_{\alpha}\, s^{\alpha}\left(\hat{\rho}^{\alpha} - \rho_i\right)_-$$

and $\beta_+ = \beta_- = 1$. Thus in (7) we get $\rho^{\alpha} = \hat{\rho}^{\alpha}$ and theorem 2 is proved.

Remark : The construction of a grid satisfying the requirements of the theorem 2 is not easy. A rectangular or triangular mesh will do it, decomposing the cell with respect to its mass center and the midle of the edges. In section III we give a more complicated example where this is satisfied.

II. KINETIC SOLVER FOR GAS DYNAMICS

The purpose of this section is to show how a kinetic solver can be implemented together with the interpolation procedure of section I in order to keep the non-negativity property of the density and pressure in gas dynamics equations, under a precise CFL condition that we will elaborate rigorously. This is achieved for the scheme we obtain in neglecting the corners ; thus, the multidimensional effect is only taken into account at the level of the kinetic upwinding.

For a rectangular mesh, the corners effects can be taken into account easily, because the piecewise constant functions on subcells lead exactly to the same situation than in a first order scheme, thus leading to the corners effects described in [9] . The point is that on a rectangular mesh the transport equation $\partial_t f + \xi \cdot \nabla_x f = 0$ can be solved exactly, and the $\int_{\mathbb{R}^p}$-integration performed exactly too. This is no longer possible on a more general grid. Therefore we prefer to neglect the corners ; the numerical tests we have performed show that, after our second order reconstruction, they indeed do not play any role. Also, using the corners leads to scheme which depends explicitely upon Δt, and thus it is no longer possible to get second order accuracy in time by the Runge-Kutta method.

In the first subsection below, we describe the "simplified" Boltzmann solver and then we prove that, under a classical CFL condition, the density and pressure remain non-negative.

II.1. Description of the scheme

After the reconstruction in subcells C_i^α of values U_i^α in section I, we use the formula (2), which requires to compute the flux $\ell_p F_p \cdot n_p$ through the edge E_p. This edge separates two cells C_i, C_j and $E_p = \left(N_i^\alpha, N_i^{\alpha+1}\right) = \left(N_j^\beta, N_j^{\beta+1}\right)$ as shown in figure 3. We compute the flux as mentioned in Corollary 3 to get the second order accuracy

$$(15) \qquad F_p \cdot n_p = \left(F\left(V_i^\alpha, V_j^\beta\right) + F\left(V_i^{\alpha+1}, V_j^{\beta+1}\right) \right) \cdot n_p/2 \ .$$

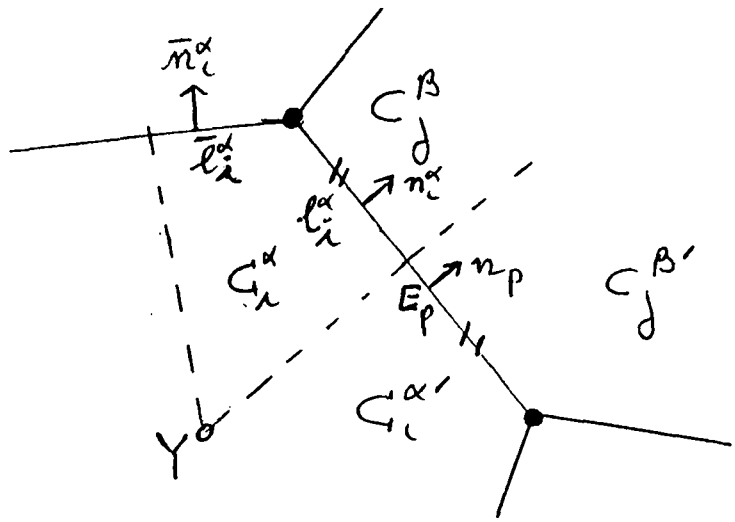

Figure 3. *Computation of the flux* $F_p \cdot n_p$

Writing (15), we have in mind that the subcells C_i^α , $C_i^{\alpha+1}$ separate E_p into two equal pieces, which is the case for rectangular or triangular grids as well as for the dual mesh we describe in section III.

Therefore the scheme will be entirely described if we give $f(U,V)\cdot n$ in (15). The kinetic formula for that, is a flux decomposition, analogous to Van Leer's scheme [15] (see also Harten-Lax-Van Leer [6]), but naturally multidimensional

$$F(U,V)\cdot n = F^+(U)\cdot n + F^-(V)\cdot n \tag{16}$$

with (setting $u = (u_1, u_2)$)

$$F^+(U)\cdot n = \rho \int_{\{\xi\cdot n \geq 0\}} \xi\cdot n \begin{pmatrix} 1 \\ \xi \\ |\xi|^2/2+\lambda T \end{pmatrix} \chi\left(\frac{\xi-u}{\sqrt{T}}\right) \frac{d\xi}{T} \tag{17}$$

and F^- is obtained changing ≥ 0 in ≤ 0 in the integration. Here $\xi \in \mathbb{R}^2$ and λ is related to γ in the pressure law (6) by

$$\lambda = \frac{1}{2}\,(2-\gamma)/(\gamma-1) \,. \tag{18}$$

The motivations for introducing these fluxes is given in [9] and we just recall that the χ function has to be choosen with the properties that it is an even, non-negative function. We also ask that

$$(19) \qquad \int_{\mathbb{R}^2} (1,\ w_k,\ w_k w_\ell)\ \chi(w)dw = (1, 0, \delta_{k\ell}) .$$

This implies the consistancy of the scheme (17) with gas dynamics i.e. $F(U,U)\cdot n = F(U)\cdot n$. Here we use the function

$$(20) \qquad \chi(w) = \frac{1}{4\pi}\ \mathbb{1}_{|w|\leq 2},$$

to get a really multidimensional upwind scheme, but

$$(21) \qquad \chi(w) = \frac{1}{12}\ \mathbb{1}_{|w_1|\leq \sqrt{3}}\ \mathbb{1}_{|w_2|\leq \sqrt{3}}$$

seems natural on rectangular mesh.

Notice that in both cases the exact integration of (17) is an easy matter while the physically relevant function $\chi(w) = \frac{1}{2\pi}\ \exp(-|w|^2/2)$, as used by Deshpande [3], Pullin [10] requires error functions. Also Kaniel [7] uses functions with bounded support for isentropic flows.

II.2. Stability analysis.

We now give a new proof of the non-linear stability of the scheme (17) ; by our second order approach, this reduces mainly to a first order analysis. We give a new proof, more direct than that of [9], and which applies to the general situation of figure 3.

Theorem 4. The scheme given by (2) with fluxes defined by (15) - (18) and (20), preserves the non-negativity of the density and pressure under the CFL condition

$$(22) \qquad \left(|u_i^\alpha| + 2\sqrt{T_i^\alpha}\right)\Delta t \leq \text{area}\left(C_i^\alpha\right) / L_i^\alpha$$

where $L_i^\alpha = \ell_i^\alpha + \bar{\ell}_i^\alpha$ (see figure 3) and $|u_i^\alpha| = \left[\left(u_{1,i}^\alpha\right)^2 + \left(u_{2,i}^\alpha\right)^2\right]^{1/2}$.

Remarks : 1) Approximately $L_i^\alpha = h$ where h is the minimal size of the edges of the cell C_i ; thus our second order approach gives a stability condition which imposes to take Δt of the same order as for the first order scheme. In that case, the CFL condition is

$$(23) \qquad \left(|u_i| + 2\sqrt{T_i}\right)\Delta t \leq \text{area}\left(C_i\right) / L_i$$

where L_i is the perimeter of the cell C_i, and $\sum_\alpha s_i^\alpha = \text{area}\left(C_i\right)$, $\sum_\alpha L_i^\alpha = L_i$.

2) For a rectangular mesh and the upwinding (22) adapted to the axes of the mesh, the CFL condition would be, for the second order scheme,

$$(24) \qquad \left(|u_{1,i}| + \sqrt{3T_i}\right)\Delta t \leq \frac{\Delta x}{2} \ , \ \left(|u_{2,i}| + \sqrt{3T_i}\right)\Delta t \leq \frac{\Delta y}{2} \ .$$

3) Also we would like to point out that, thanks to corollary 3, the full scheme is second order accurate in space. Second order accuracy in space and time could be obtained using a Runge-Kutta method while keeping the theorem 4 (see Khobalatte and Perthame [8], a multidimensional study of the entropy condition can also be found therein).

Proof of theorem 4.

First step : Kinetic equation. We have to prove that if all the subvalues $\rho_i^{\alpha,n}$, $T_i^{\alpha,n}$ are non-negative at time t_n , they remain non-negative at time t_{n+1} . Following the Boltzmann type of approach we define the kinetic values, for $\xi \in \mathbb{R}^2$,

$$f_i^{\alpha,n}(\xi) = \rho_i^{\alpha,n} \ \chi\left(\frac{\xi - u_i^{\alpha,n}}{T_i^{\alpha,n}}\right) \Big/ T_i^{\alpha,n}$$

and $f^{n+1}(\xi)$ is defined by a formula analogous to (2) for f (we have in mind that f should solve $\partial_t f + \xi \cdot \nabla_x f = 0$, and we write a numerical approximation of this free transport equation)

$$(25) \qquad \text{area}\,(C_i)\ f_i^{n+1}(\xi) - \sum_\alpha f_i^{\alpha,n}(\xi)\ s_i^\alpha + \Delta t \sum_\alpha \left[(\xi \cdot n_i^\alpha)_+ \ell_i^\alpha + (\xi \cdot \bar{n}_i^\alpha)_+ \bar{\ell}_i^\alpha\right] f_i^{\alpha,n}(\xi)$$

$$= \Delta t \sum_\beta \left[\left(\xi \cdot n^\beta\right)_- \ell^\beta\ f^{\beta,n}(\xi)\right] .$$

Here the summations over α are taken for subcells of C_i ; n_i^α and $\bar{n}_i^\alpha$ are the outward normals to the two edges of C_i^α as in figure 3, with length ℓ_i^α , $\bar{\ell}_i^\alpha$. The summation over β, is taken for all subcells $C_{j(\beta)}^\beta$ neighboring C_i and we omit the index $j(\beta)$, n^β is the outward normal to the corresponding subcell $C_{j(\beta)}^\beta$.

Second step : Non-negativity of f^{n+1} . In order to check that $f_i^{n+1}(\xi) \geq 0$, we just have to check that for all i, α

$$(26) \qquad s_i^\alpha - \Delta t \left[\left(\xi \cdot n_i^\alpha \right)_+ \ell_i^\alpha + \left(\xi \cdot \bar{n}_i^\alpha \right)_+ \bar{\ell}_i^\alpha \right] \geq 0 .$$

But we only consider values of ξ such that $f_i^{\alpha,n}(\xi) > 0$, i.e. $|\xi - u_i^\alpha| \leq 2\sqrt{T_i^\alpha}$, and thus (26) will hold as soon as the CFL condition (22) is achieved.

Third step : Back to gas dynamics. We now fix $\gamma = 2$ so that $\lambda = 0$, the general case being treated exactly as in [9]. Then we recover (2) from (25) by setting

$$U_i^{n+1} = \int_{\mathbb{R}^2} \left(1, \xi, |\xi|^2/2\right)^t f_i^{n+1}(\xi)\, d\xi ,$$

and noticing that, thanks to the relations (19)

$$U_i^{\alpha,n} = {}^t(\rho, \rho u, E)_i^{\alpha,n} = \int_{\mathbb{R}^2} \left(1, \xi, |\xi|^2/2\right)^t f_i^{\alpha,n}(\xi)\, d\xi .$$

Thus integrating (25) $d\xi$ against the vector $\left(1, \xi, |\xi|^2/2\right)^t$, we find exactly (2) with the flux relations (16) - (17) . Since $f^{n+1}(\xi) \geq 0$ for all ξ, we find that $\rho_i^{n+1} \geq 0$ and also $(\rho T)_i^{n+1} = \int |\xi - u_i^{n+1}|^2 f_i^{n+1}(\xi)\, d\xi \geq 0$.
This proves theorem 4.

Remark : Since we solve in fact the transport linear equation, when we impose that the scheme is conservative and preserves $f \geq 0$, we also impose a TVD property for $f(\xi)$ and a fixed ξ .

III. UNSTRUCTURED MESH

We now describe an example of unstructured mesh where our method can be completely implemented, thus leading to a second order accurate code that preserves non-negativity. This mesh has already been used with unsignificant differences, by Angrand, Dervieux, Boulard, Periaux, Vijayasundaram [1], Rostand, Stouflet [12].

The basis of the mesh is a triangulation with vertices X_i , and the cells C_i are obtained by joining the mass centers of the triangles as shown in figure 4. It has to be noted that the mass center x_i of the cell C_i is not usually X_i . We will assume that our triangulation is smooth enough so that all the triangles $\left(N_i^\alpha,\ N_i^{\alpha+1},\ x_i\right)$, built with the vertices of the cell C_i are contained in C_i itself. The points N_i^α are here mass centers of the primal triangles.

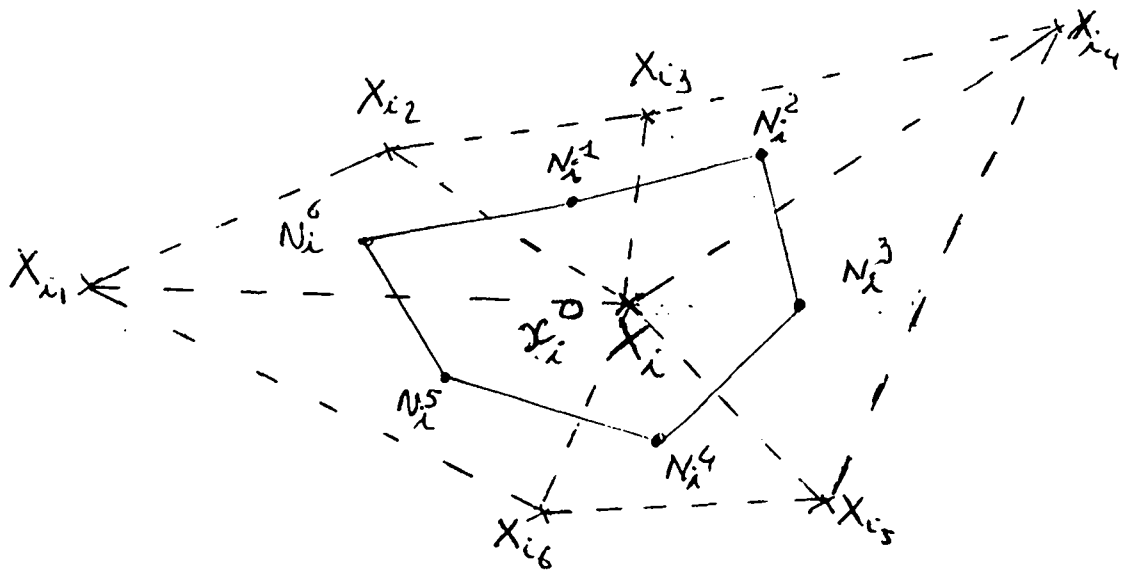

Figure 4. The control volume $C_i(\cdot)$ is deduced from the triangles (x) . It is used as in figure 3 to solve the gas dynamics equations.

The details of the implemention of the scheme are described precisely in Y.Qiu [11]. Let us just point out that for second order accuracy, we have to find values $V\left(N_i^\alpha\right)$. Since the averages are known at the center of mass x_i,

and not at the points X_i, we have to keep in the computer memory the barycentric coordinates of the points N_i^α with respect to the three associated points x_i, x_{i_1}, x_{i_2} (these coordinates would be 1/3, 1/3, 1/3 if $x_i = X_i$, $x_{i_1} = x_{i_1}$, $x_{i_2} = X_{i_2}$). Then, the value $V(N_i^\alpha)$ is interpolated with these coefficients and limited so as to satisfy the requirements (14) for non-negativity of T_i^α. The areas s_i^α are also kept in memory (one by edge of a triangle), again these areas have been computed with respect to the mass center x_i. With these notations we can check the conditions of theorem 2 for second order accuracy.

Proposition 5. The relation (3) holds for the dual mesh of figure 4.

Proof of Proposition 5. Considering the vertices $(N^\alpha)_{1\le\alpha\le\alpha_M}$ (we drop the index i) let us introduce the mass center y^α of the triangle $K^\alpha = \left(x_\lambda, N^\alpha, N^{\alpha+1}\right)$, identifying N^{α_M+1} and N^1. We have

$$(27) \qquad y^\alpha = \left(x+N^\alpha + N^{\alpha+1}\right)/ 3 , \qquad \sigma^\alpha y^\alpha = \int_{K^\alpha} x\, dx ,$$

where σ^α = area (K^α). Since $\sum_\alpha \sigma^\alpha$ is the area $|C|$ of the cell C we find

$$|C|\ x_\lambda = \int_C x\, dx = \sum_\alpha \sigma^\alpha y^\alpha$$

$$= \sum_\alpha \sigma^\alpha \left(N^\alpha + N^{\alpha+1}\right) / 3 + |C|x_\lambda / 3,$$

$$|C|\ x_\lambda = \sum_\alpha \sigma^\alpha\left(N^\alpha + N^{\alpha+1}\right) / 2$$

$$= \sum_\alpha s^\alpha N^\alpha$$

because $s^\alpha = \left(\sigma^\alpha + \sigma^{\alpha-1}\right) / 2$, and proposition 5 is proved.

IV. NUMERICAL RESULTS

We now present three numerical tests we have performed on the unstructured mesh of section III. Except the first one, our tests concern stationary hypersonic flows where negative pressures could arise either low density zones or rapid changes in the first iterations of the transient regime.

IV.1. Reflexion problem - This problem can be found in [2] . We have used two different grids. A 60x20 rectangular grid and a triangular grid deduced from the first one.

IV.2. Double ellipse problem - The mesh around the double ellipse contains 2258 nodes. The incidence is 30° and the mach number 8.15. We have taken γ=1.4 to fit the Hermes test problem [5]. We have observed a fluctuation on the enthalpy of approximately 2.5% out of the shock.

IV.3. Flow around an ellipse - We now consider a global calculation around an ellipse. The mesh contains 3630 nodes. The incidence is 30°, the mach number 25, γ=1.2. We have observed a fluctuation on the enthalpy of approximately 4.0% out of the shock.

Further details and numerical results can be found in [11] .

Acknowledgment. The authors wish to thank P. Le Tallec and M. O. Bristeau for fruitful discussions.

REFERENCES

[1] **F. Angrand, A. Dervieux, V. Boulard, J. Periaux and G. Vijayasundaram.** Transonic Euler Simulations by means of finite Element Explicit Schemes. AIAA - 83 - 1924.

[2] **P. Colella.** Multidimensional upwind methods for hyperbolic conservation laws. J.C.P. 87, (1990) p. 171-200.

[3] **S. Deshpande.** A second order accurate, kinetic theory based, method for inviscid compressible flows. NASA Technical paper n° 2613 (1986).

[4] **L.J. Durlofsky, B. Engquist, S. Osher.** Triangle Based TVD Schemes for Hyperbolic Conservations Laws. CAM report 89-33, UCLA.

[5] **Hermes** Workshop. Antibes (1991). To appear.

[6] **A. Harten, P.D. Lax and B. Van Leer.** On upstream differencing and Godunov type schemes for hyperbolic conservation laxs, SIAM Review, 25 (1983), p. 35-61.

[7] **S. Kaniel.** A kinetic model for the compressible flow equations. Indiana Univ. Math. J. 37(3) (1988), p. 537-563.

[8] **B. Khobalatte and B. Perthame.** In preparation.

[9] **B. Perthame.** Second order Boltzmann schemes for compressible Euler Equations in one and two space variables. To appear in SIAM J. num. Anal.

[10] **D.I. Pullin.** Direct Simulation methods for compressible Inviscid-Ideal-Gas-Flow. J.C.P. 34 (1980) p. 231-244.

[11] **Y. Qiu.** Thesis in preparation, Un. P6, and INRIA report n°

[12] **P. Rostand and B. Stoufflet.** TVD schemes to compute compressible viscous flows on unstructured meshes, in Notes on Numerical Fluid Mechanics, 24, p. 510-520, J. Ballmann and R. Jeltsch, eds., Vieweg, Weisbaden (1988).

[13] **R. Sanders and A. Weiser.** A high order staggered grid method for hyperbolic systems of conservation laws. Math. Comp.

[14] **B. Van Leer.** Towards the Ultimate Conservative Difference Scheme. V, A second order sequel of Godunov's method. J.C.P. (1979), p. 101-136.

[15] **B. Van Leer.** Flux vector splitting for the Euler Equations. 8th international on numerical methods in fluid dynamics, Krause Ed., pp 507-512, Lecture note in physics, 170, Springer-Verlag (1982)

[16] **B. Cockburn and C.W. Shu.** T.V.B. Runge-Kutta local projection discontinuous Galerkin finite element method for conservation laws II : General framework, Math. Comp. 52 (1989), p. 411-435.

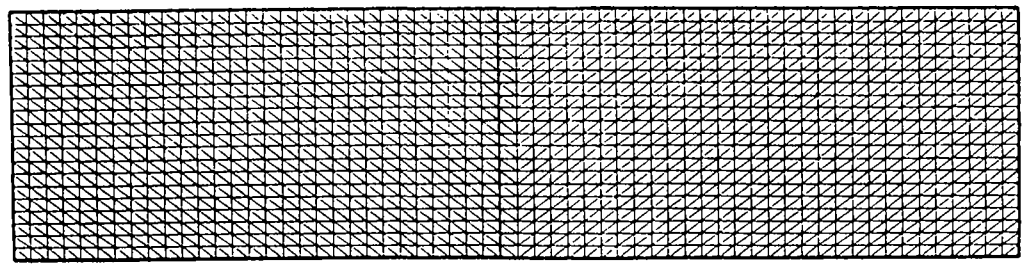

Figure 5.1 Finite element mesh, 1281 nodes, 2400 elements

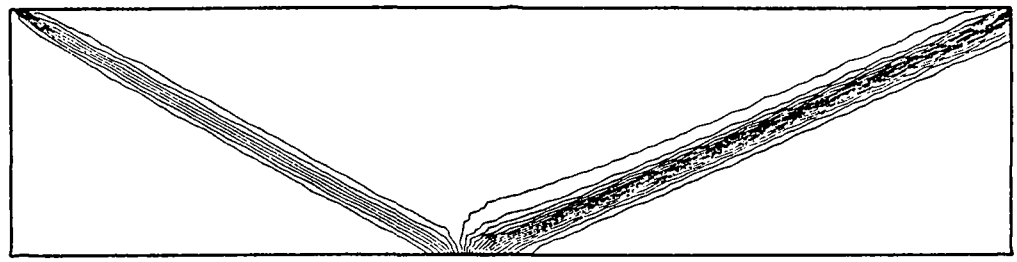

Figure 5.2 Iso-pressure lines, Min=0.71, Max=2.94, 25 contour lines

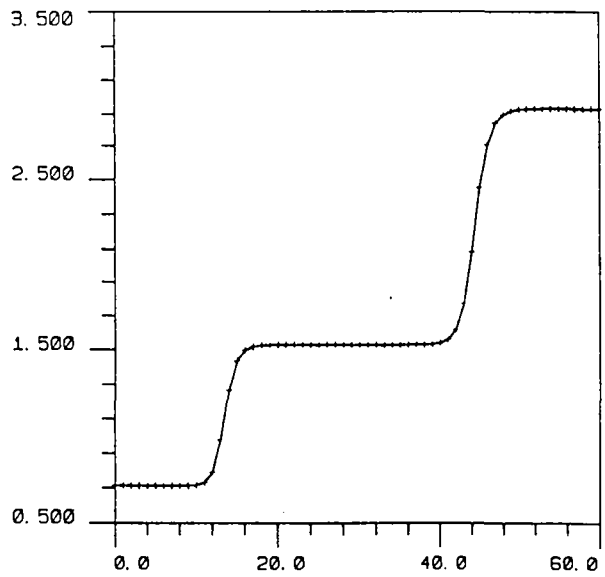

Figure 5.3 Pressure on center-line as a function of horizontal dimension (x)

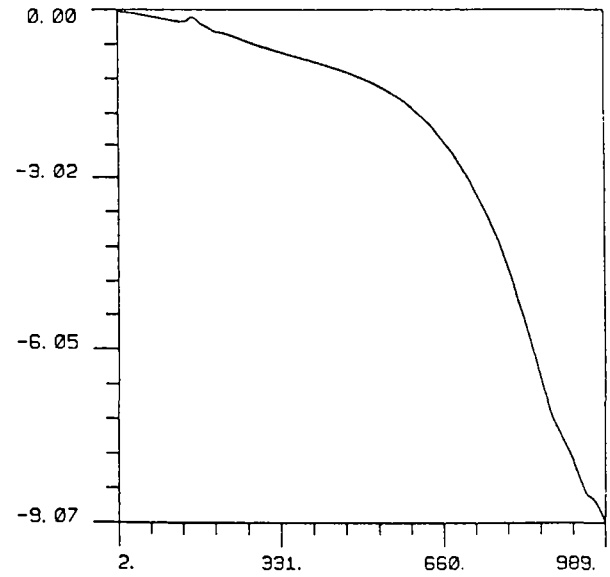

Figure 5.4 Convergence history logarithm of error $\Sigma_i |\, \S_i^{n+1} - \S_i^n \,|$ vs number of iterations

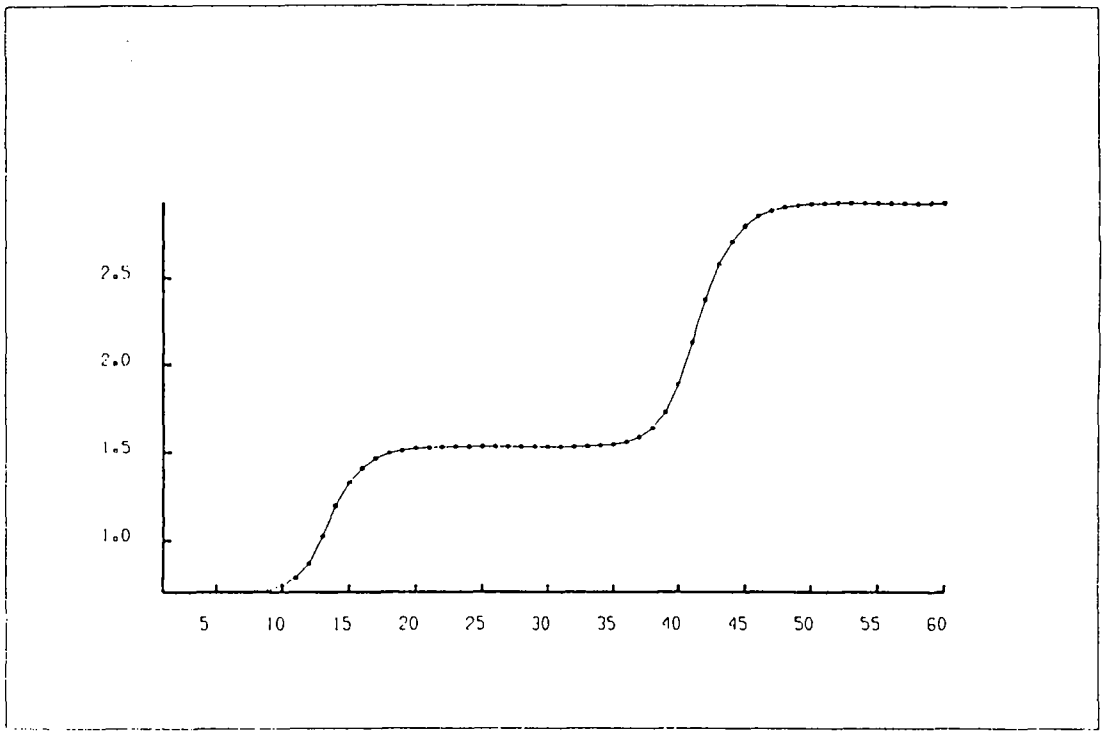

Figure 5.5 Pressure on center-line as a function of horizontal dimension (x), for rectangular mesh

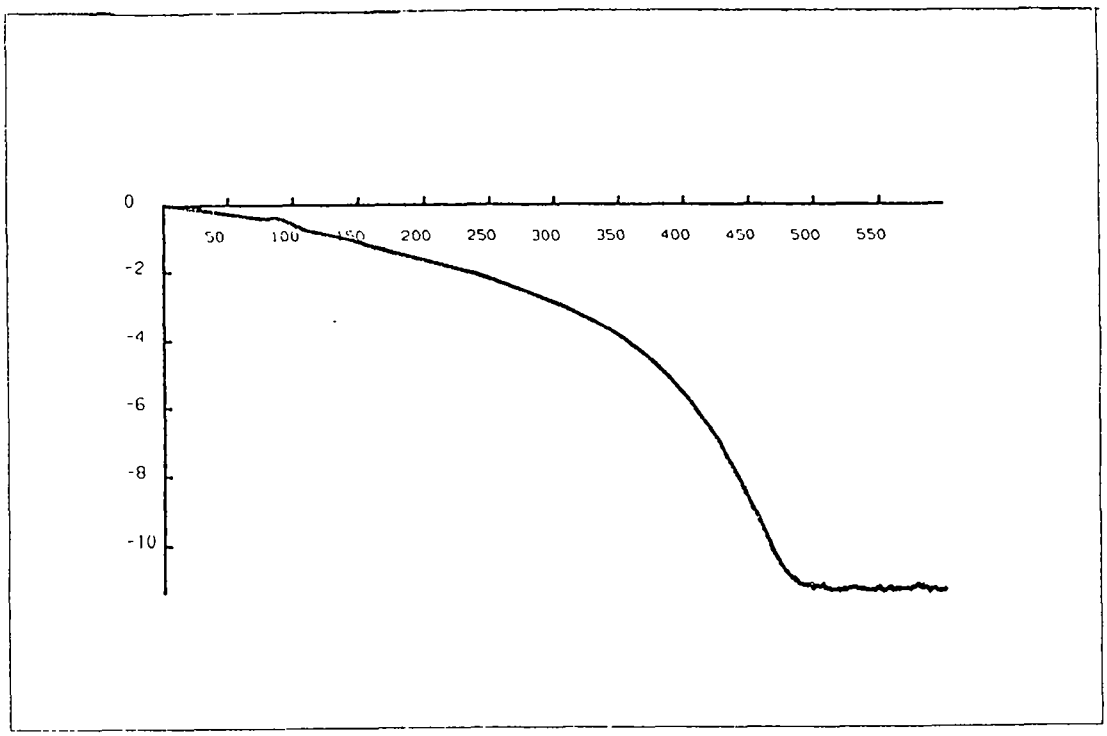

Figure 5.6 Convergence history logarithm of error $\Sigma_i | S_i^{n+1} - S_i^n |$ vs number of iterations , for rectangular mesh

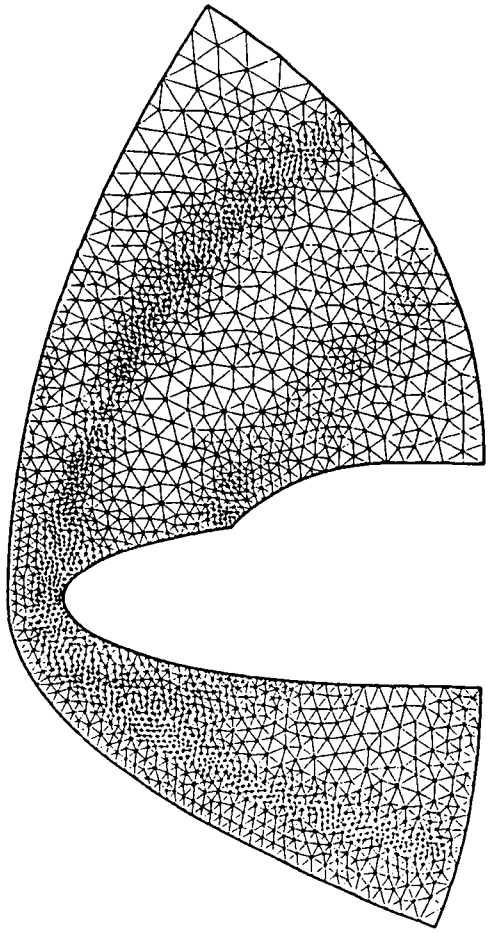

Figure 6.1 Finite element mesh
2258 nodes, 4295 elements

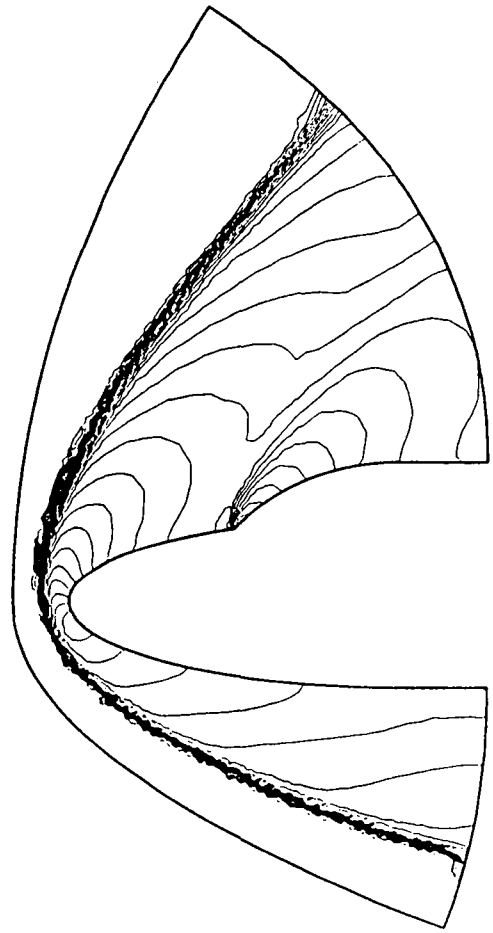

Figure 6.2 Iso-Mach number lines
Min=0.03, Max=8.15, 30 contour lines

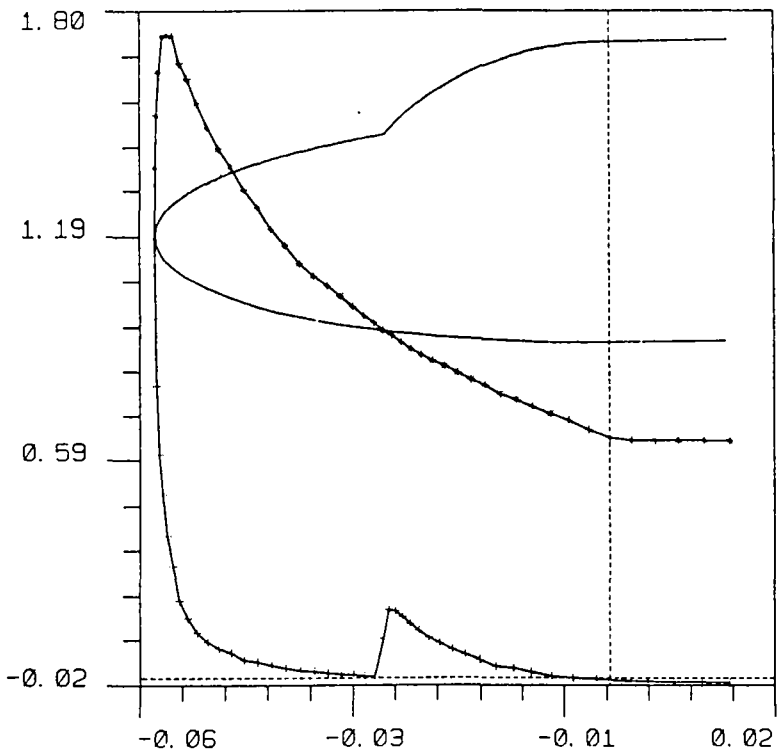

Figure 6.3 Cp Wall distribution

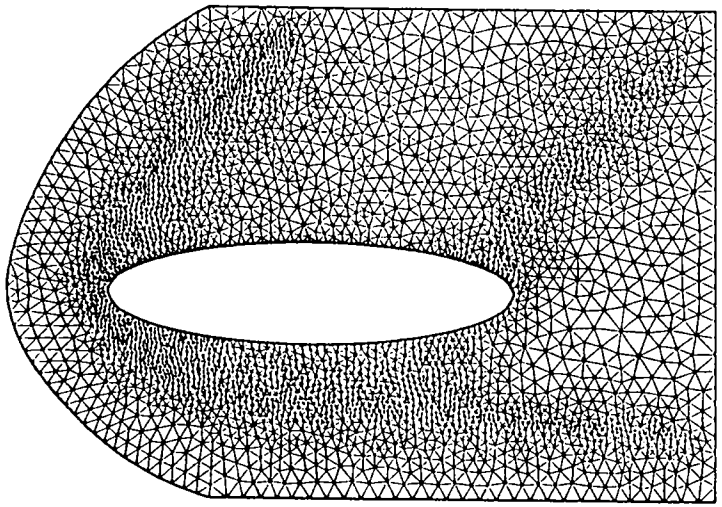

Figure 7.1 Finite element mesh
3630 nodes, 6970 elements

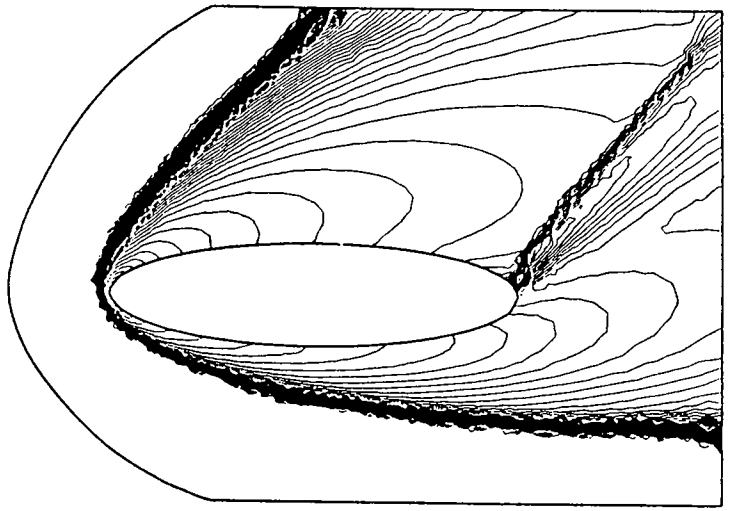

Figure 7.2 Iso-Mach number lines
Min=0.04, Max=25.0, 100 contour lines

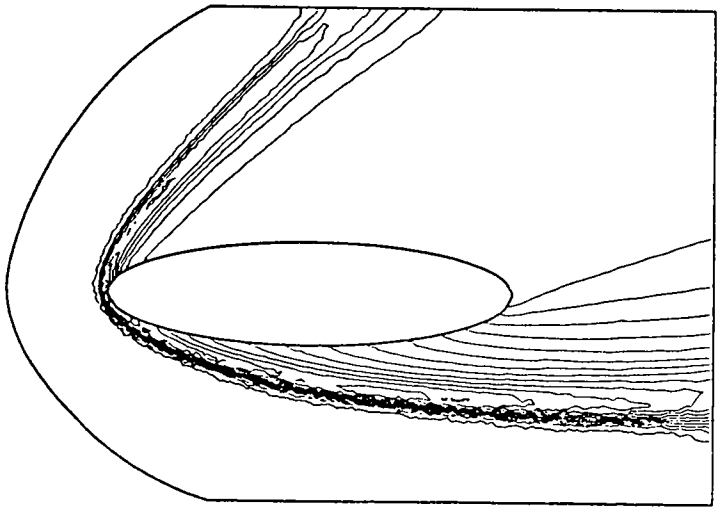

Figure 7.3 Iso-density lines
Min=0.05, Max= 10.06, 20 contour lines

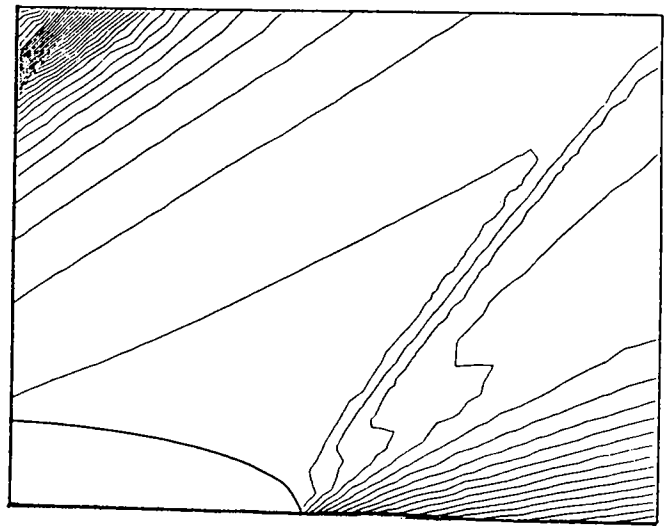

Figure 7.4. Iso-Density lines
behind the obstacle

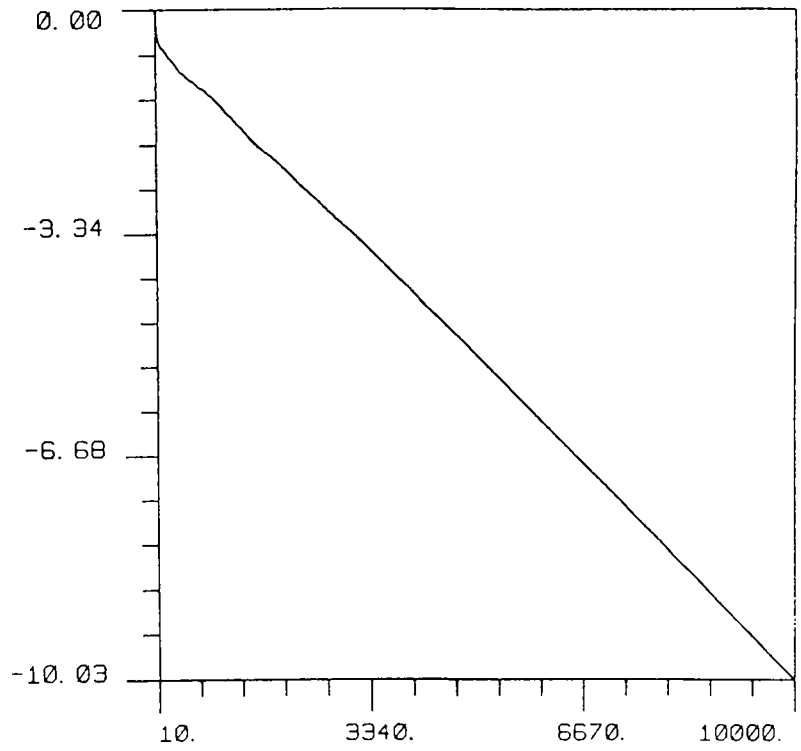

Figure 6.4 Convergence history logarithm of error $\Sigma_i |\rho_i^{n+1} - \rho_i^n|$ vs number of iterations, for problem IV.2.

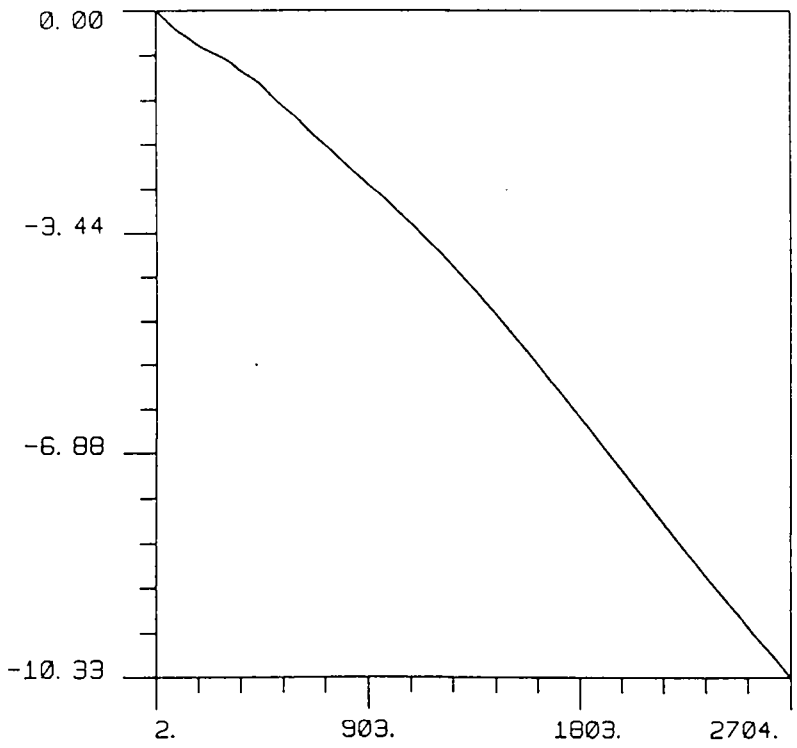

Figure 7.5 Convergence history logarithm of error $\Sigma_i |\rho_i^{n+1} - \rho_i^n|$ vs number of iterations, for problem IV.3.

ISSN 0249-6399